

Chemical Science

Topological isomerism in a chiral handcuff catenane

Karel J. Hartlieb,^a Anthea K. Blackburn,^a Severin T. Schneebeli,^a Ross S. Forgan,^a
Amy A. Sarjeant,^a Charlotte L. Stern,^a Dennis Cao,^a and J. Fraser Stoddart^{*a}

^a*Department of Chemistry, Northwestern University, Evanston, IL 60208, USA.
E-mail: stoddart@northwestern.edu*

SUPPORTING INFORMATION

Table of Contents

S1.	2D ¹H NMR Spectroscopy	S1
S2.	Variable-Temperature ¹H NMR Spectroscopy	S9
S3.	X-Ray Crystal Structure Data	S11
S4.	Quantum Mechanical Calculations	S13
S5.	Analytical Reverse-Phase HPLC	S20
S6.	Isothermal Titration Calorimetry Data	S21
S7.	References	S22

S1. 2D ^1H NMR Spectroscopy

Through analysis of 2D ^1H NMR spectra, it is possible to assign partially resonances to the protons of the handcuff catenane (Figure S1). The protons α to the nitrogens on the bipyridinium units can be related (Figure S2) to their vicinal protons β to the nitrogens on the bipyridinium units by 2D COSY NMR spectroscopy. Two-bond correlations can also be established between protons $\text{H}_{\text{A-H}}$ residing on methylene carbons (Figure S3), and three-bond correlations can be observed (Figures S3 and S4) between protons *ortho* to each other on the DNP units. We conclude that $\text{H}_{\alpha 1}$ and $\text{H}_{\alpha 7}$ are present on the same pyridinium ring; the same can also be said for $\text{H}_{\alpha 2/6}$, $\text{H}_{\alpha 3/4}$ and $\text{H}_{\alpha 5/8}$, which are established by four-bond correlations (Figures S5 and S6) between the two α or the two β protons on the same pyridinium ring, as well as the presence of through-space correlations (Figure S7), observed from 2D ROESY NMR spectra, between the methylene $\text{H}_{\text{A-H}}$ and α protons. Through-space correlations (Figure S8) between H_{i4} and H_1 , and H_{i8} and $\text{H}_{2/3}$ confirm that H_{i4} is directed towards the center of the handcuff catenane, while H_{i8} points towards the terminal para-xylylene units. 2D COSY and ROESY ^1H NMR spectroscopy enabled us to identify that $\text{H}_{\alpha 2/6,3/4}$ reside in close proximity to the central benzenoid ring owing to the detection of through-space correlations between H_1 and H_B and H_D (Figure S7) that consequently display (Figure S3) through-bond correlations with H_A and H_C , respectively. These methylene protons show further through-space correlations with the protons α to the nitrogens on the pyridinium rings closest to the central benzenoid ring. The same analytical process was used to verify that $\text{H}_{\alpha 1/7,5/8}$ reside on the pyridinium rings furthest away from the central benzenoid ring.

The 2D ^1H EXSY spectra (Figures S9 and S10) reveals the presence of, not only site exchange between the α protons (and their respective β protons) on the same pyridinium ring, but also

between these protons on *opposite* sides of the cyclophane. In order to understand this phenomenon, the mechanism of the DNP reorientation has to be considered. Although the presence of the co-conformation wherein both DNP units reside in different orientations in the *meta-meta* isomer is not observed by ^1H NMR spectroscopy, it is possible for the DNP units to undergo an inversion process (Figure 8) provided they both leave the cavities of the cyclophanes, experience a pedaling motion and return inside the cavities in a concerted fashion. The co-conformations generated by this inversion process are degenerate. This degeneracy can be appreciated by rotating the original co-conformation by 180° around one of two different axes – one running through the center of the molecule intersecting all three phenylene rings, and the other one lying within the plane of the central benzenoid ring, but perpendicular to the C_2 axis shown in Figure S1. This degeneracy, which is illustrated in Figure 8, explains the site exchanges between the $H_{a1,7,5,8}$ protons (Figure S9). The site exchanges involving these protons are also mirrored more clearly between methylene protons on opposite sides of the cyclophanes, e.g., H_B and H_D are undergoing site exchange with each other (Figure S10) although 2D ^1H COSY NMR spectroscopy (Figure S3) reveals that these protons do not possess a through-bond correlation — i.e., they are not bound to the same methylene carbon — and therefore must be on opposite sides of the cyclophane, since both H_B and H_D have through-space correlations (Figure S7) with H_I .

The 2D EXSY spectra (Figures S9 and S10) also inform us that there is no site exchange between protons on the *ortho-ortho* isomer and those associated with the *meta-meta* isomer. Hence, it can be concluded that these two species are two distinct isomers that are not in equilibrium with each other. 2D DOSY (Figure S11) reveals that the *meta-meta* and *ortho-ortho* isomers have near identical diffusion properties in CD_3CN , confirming that the molecules constituting these two isomers have very similar sizes and charges.

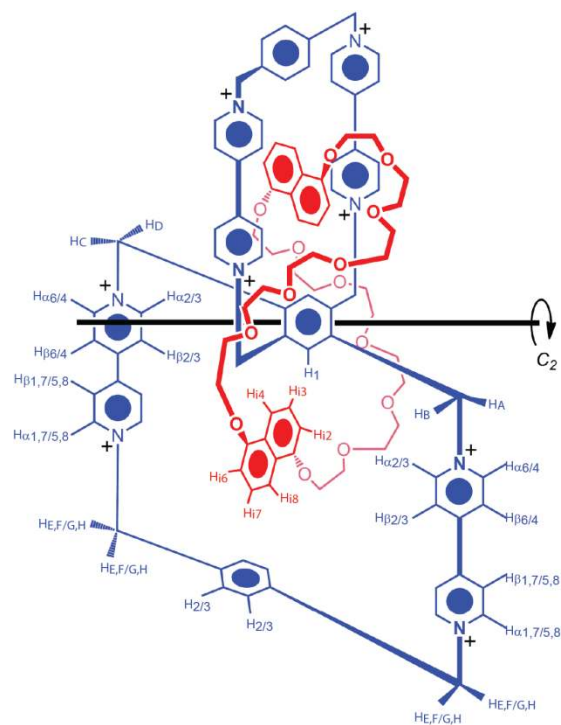


Figure S1. Structural formula of handcuff catenane HC^{8+} . Protons on the structural formula are labelled in keeping with their corresponding ^1H NMR assignments.

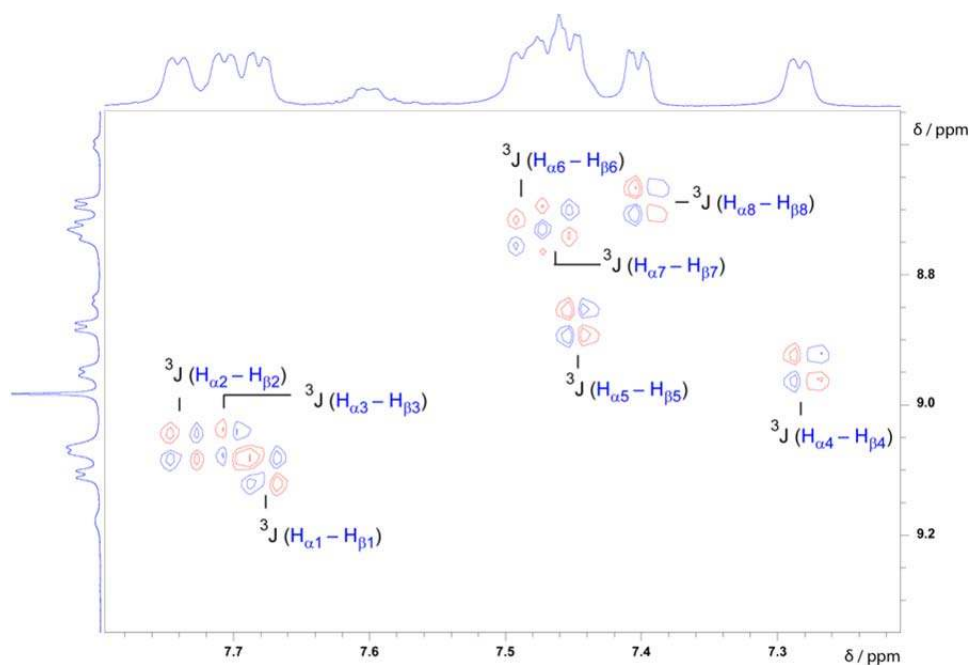


Figure S2. Partial ^1H - ^1H gDQF COSY (600 MHz, CD_3CN , 298 K) spectrum of HC^{8+} with selected correlations labelled.

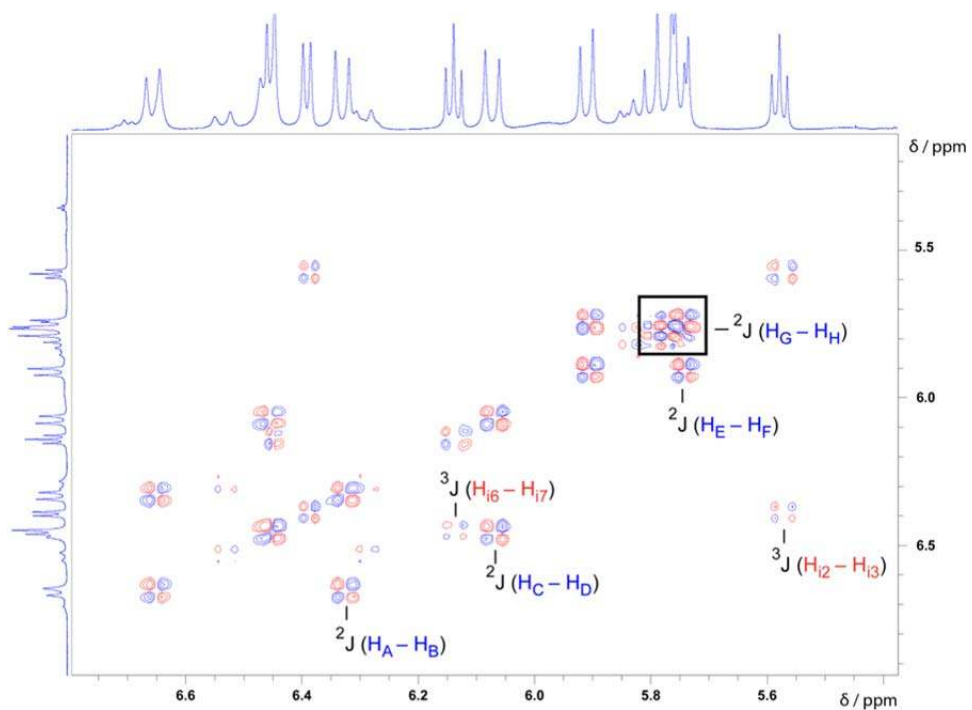


Figure S3. Partial 1H - 1H gDQF COSY (600 MHz, CD_3CN , 298 K) spectrum of $HC\cdot 8PF_6$ with selected correlations labelled.

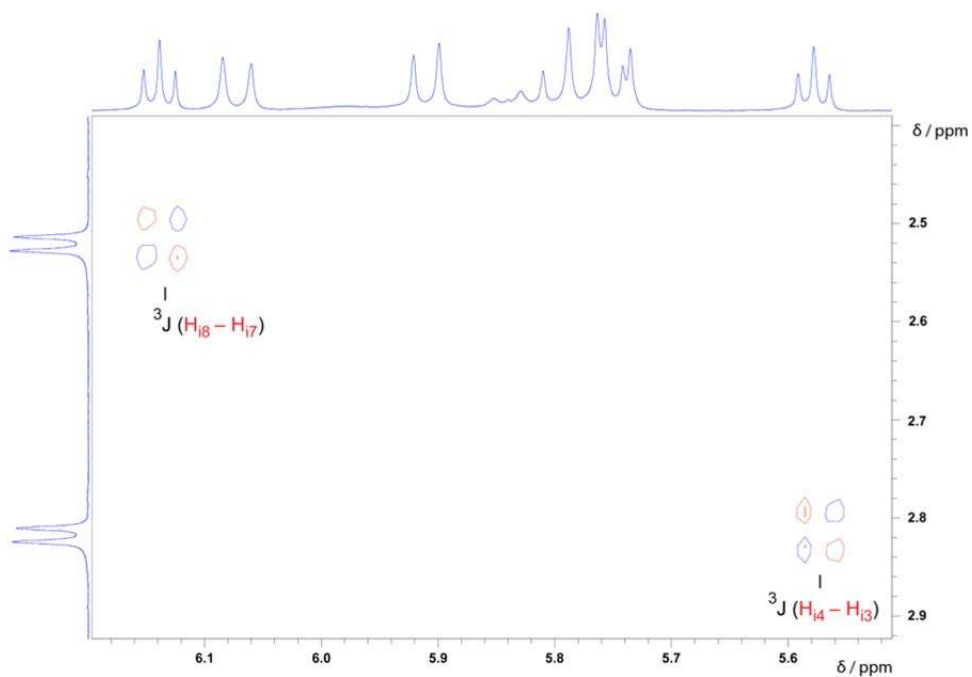


Figure S4. Partial 1H - 1H gDQF COSY (600 MHz, CD_3CN , 298 K) spectrum of $HC\cdot 8PF_6$ with selected correlations labelled.

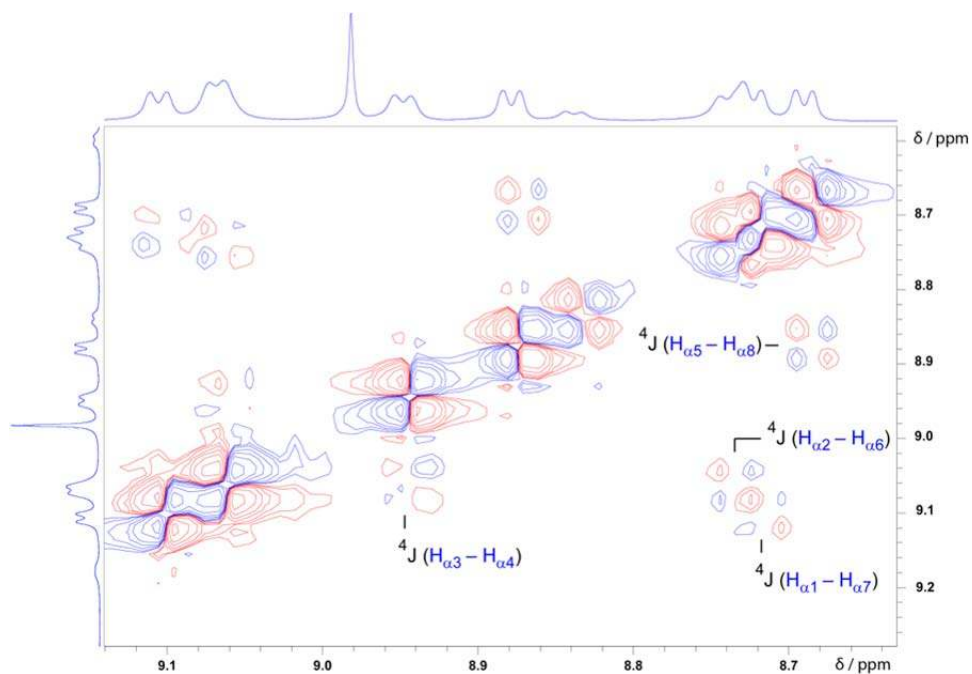


Figure S5. Partial ${}^1\text{H}$ - ${}^1\text{H}$ gDQF COSY (600 MHz, CD_3CN , 298 K) spectrum of $\text{HC}\cdot 8\text{PF}_6$ with selected correlations labelled.

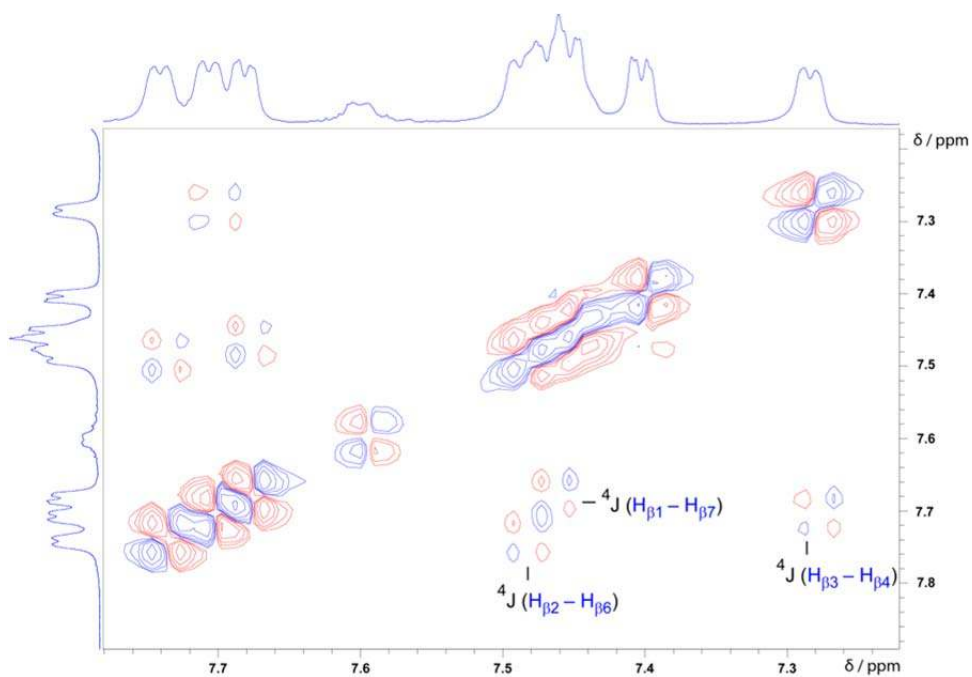


Figure S6. Partial ${}^1\text{H}$ - ${}^1\text{H}$ gDQF COSY (600 MHz, CD_3CN , 298 K) spectrum of $\text{HC}\cdot 8\text{PF}_6$ with selected correlations labelled.

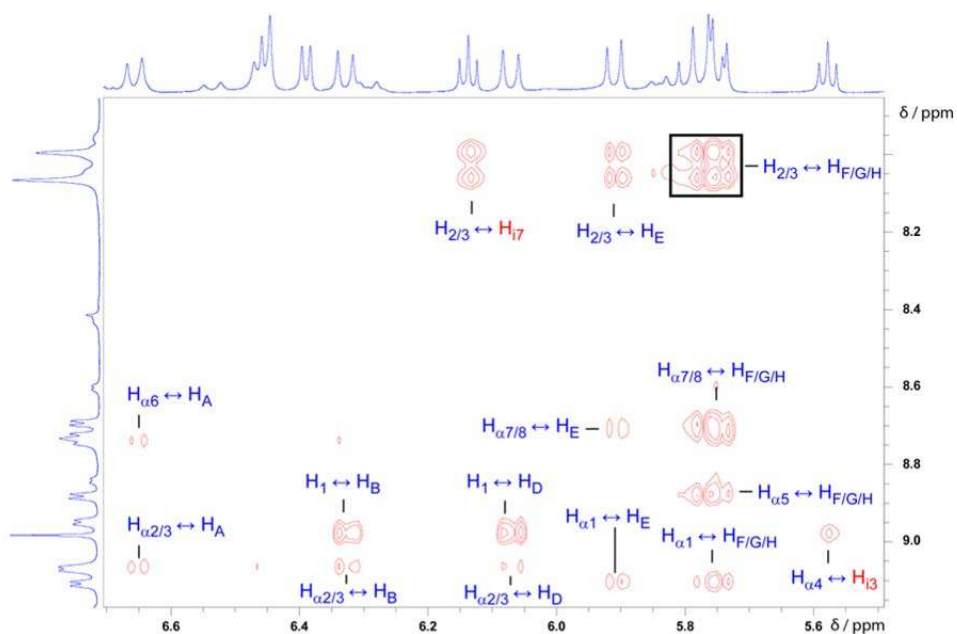


Figure S7. Partial ¹H ROESY (600 MHz, CD₃CN, 298 K) spectrum of HC•8PF₆ with selected correlations labelled.

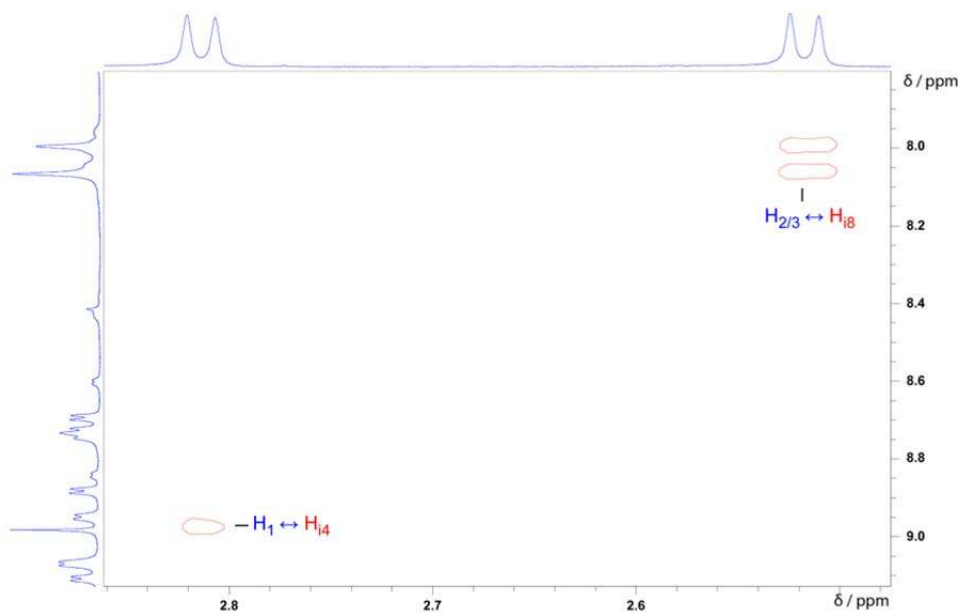


Figure S8. Partial ¹H ROESY (600 MHz, CD₃CN, 298 K) spectrum of HC•8PF₆ with selected correlations labelled.

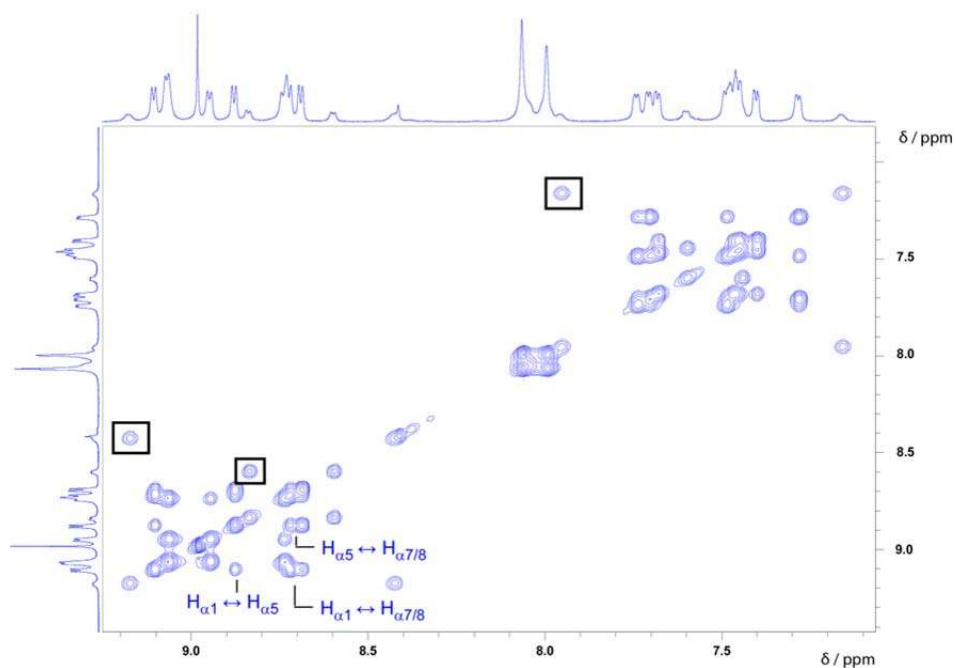


Figure S9. Partial 2D ^1H EXSY (600 MHz, CD_3CN , 298 K) spectrum of $\text{HC}\cdot 8\text{PF}_6$. Outlined crosspeaks show signals for the *ortho-ortho* isomer undergoing exchange with each other, but no signals are observed to suggest the *ortho-ortho* isomer undergoes exchange with the *meta-meta* isomer.

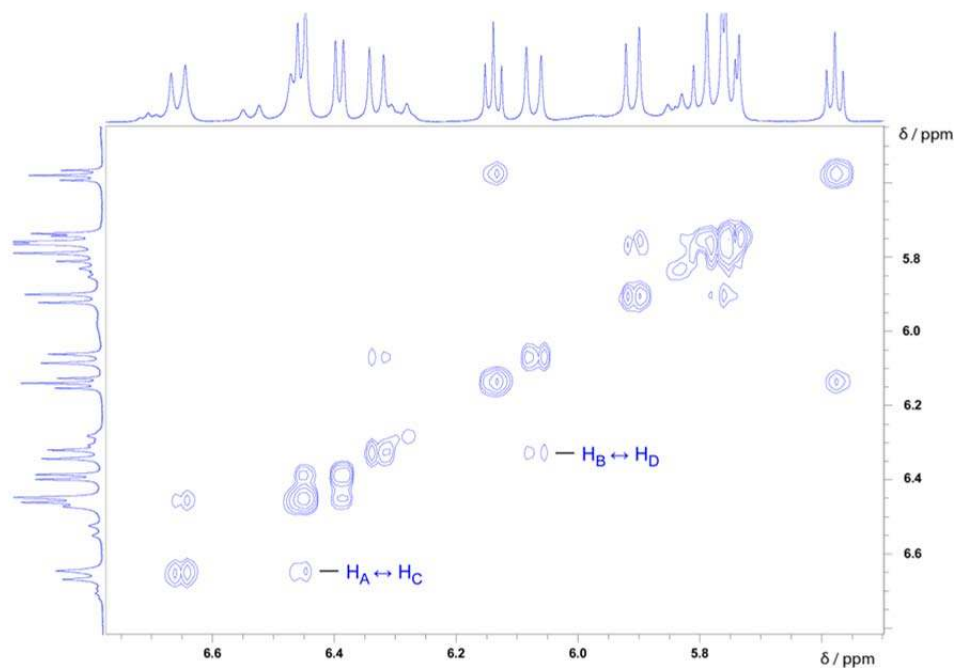


Figure S10. Partial 2D ^1H EXSY (600 MHz, CD_3CN , 298 K) spectrum of $\text{HC}\cdot 8\text{PF}_6$.

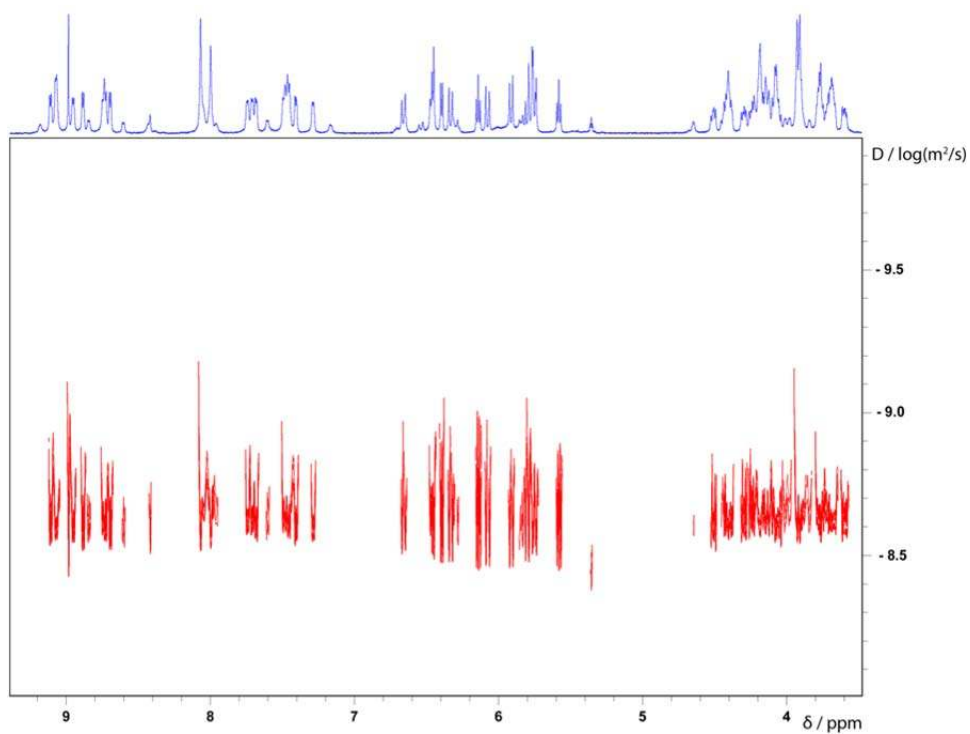


Figure S11. 2D ^1H DOSY (600 MHz, CD_3CN , 298 K) spectrum of **HC**• 8PF_6

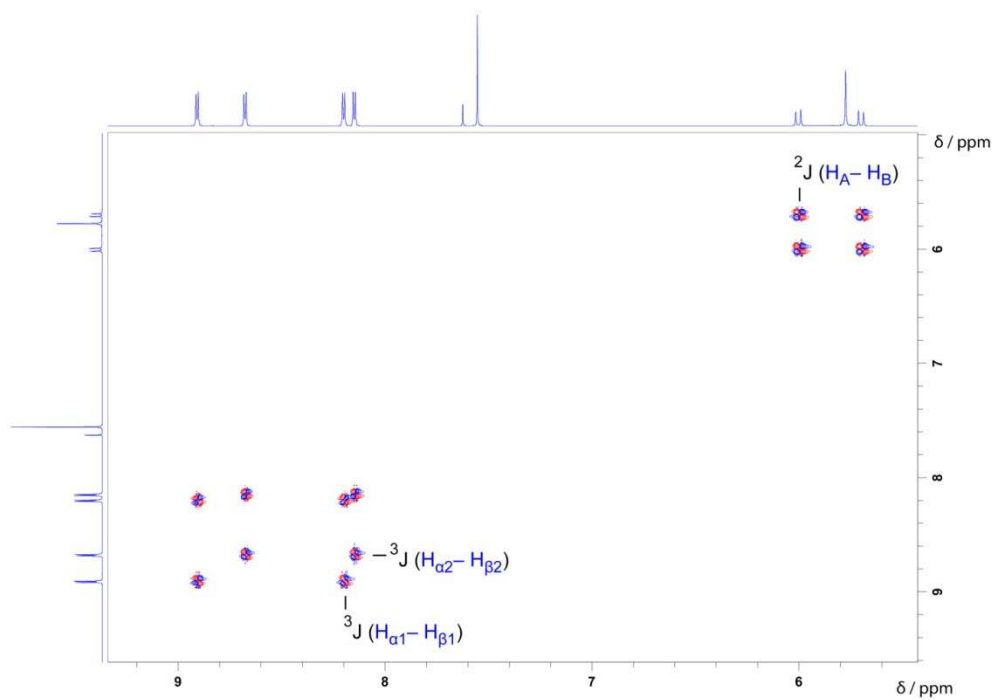


Figure S12. ^1H - ^1H gDQF COSY (600 MHz, CD_3CN , 298 K) spectrum of **DBB**• 8PF_6 with selected correlations labelled.

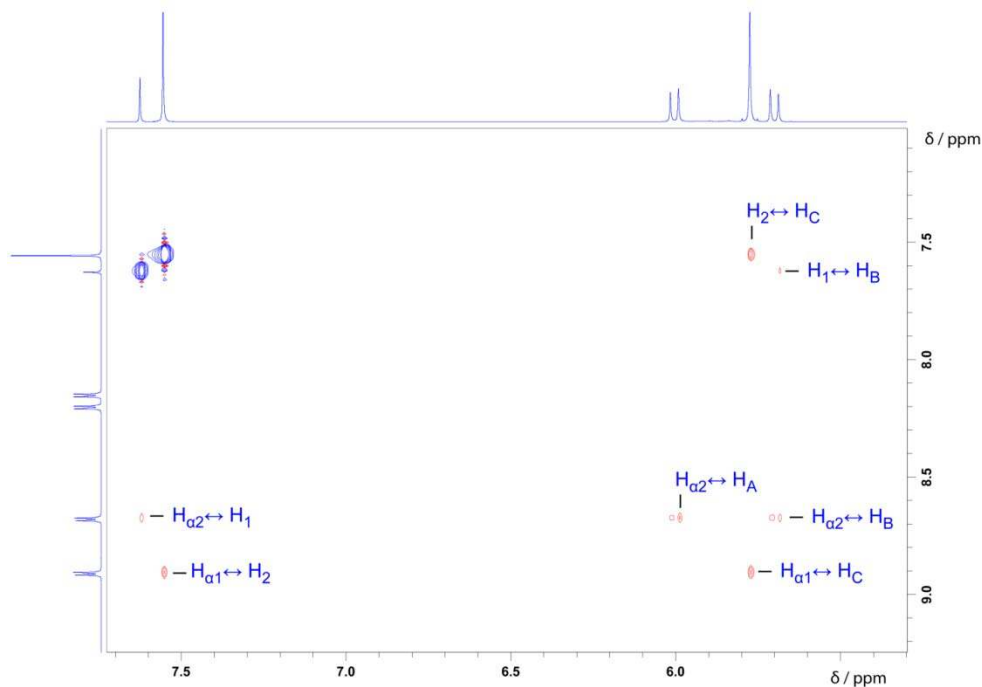


Figure S13. Partial NOESY (600 MHz, CD₃CN, 298 K) spectrum of **DBB•8PF₆** with selected correlations labelled.

S2. Variable-Temperature ¹H NMR Spectroscopy

When the handcuff catenane **HC**⁸⁺ is heated to 363 K in CD₃SOCD₃ (Figure S14), no coalescence of the resonances for the *meta-meta* and *ortho-ortho* isomers is observed, supporting our claim that these two species exist as distinct isomer that are not in equilibrium with each other. Upon cooling the sample to 233 K, the signals in the ¹H NMR spectrum remain sharp (Figure S15), suggesting that slowing of DNP reorientation does not result in the detection of two co-conformations, and therefore the relative orientations of both DNP units is restricted by the length of the polyether chains; further evidence supporting our claim that DNP reorientation occurs in a concerted manner.

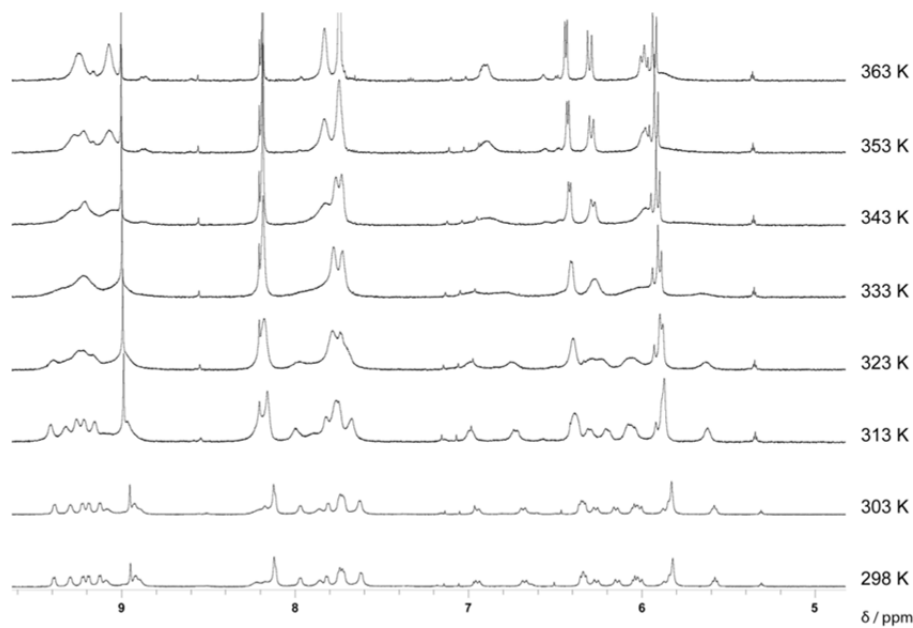


Figure S14. Partial ^1H NMR (600 MHz, $(\text{CD}_3)_2\text{SO}$) spectrum of $\text{HC}\cdot 8\text{PF}_6$. Signals for the *meta-meta* isomer appear to coalesce with increasing temperature. Signals for the *ortho-ortho* isomer, however, do not coalesce with those of the *meta-meta* isomer.

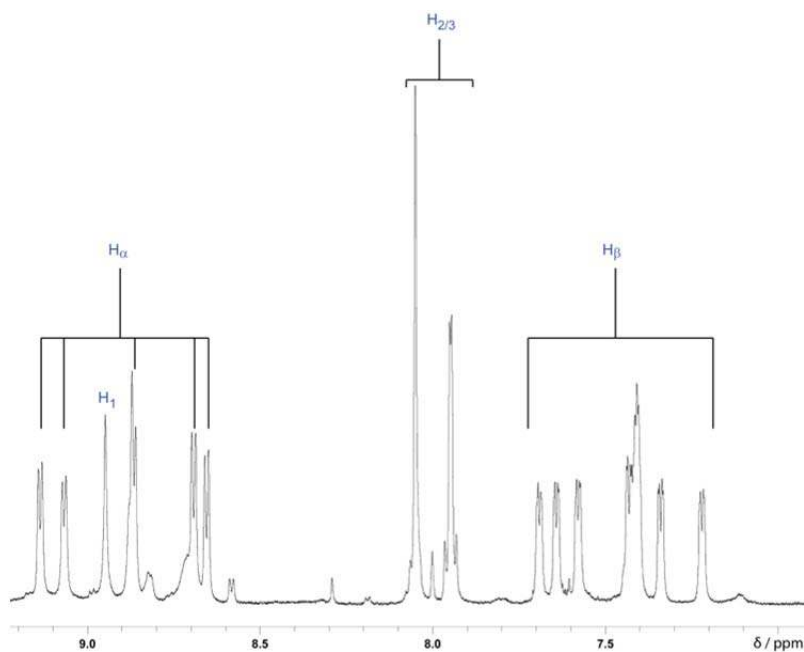


Figure S15. Partial ^1H NMR (600 MHz, CD_3CN , 233K) spectrum of $\text{HC}\cdot 8\text{PF}_6$. The signals for H_α , H_β and $\text{H}_{1,2,3}$ remain sharp, suggesting that upon cooling, two possible co-conformations of the *meta-meta* isomer that are dependent upon DNP orientation, are not in fast exchange on the ^1H NMR timescale and do not exist in solution.

S3. X-Ray Crystal Structures

Data were collected at 100 K using a Bruker d8-APEX II CCD diffractometer (Cu K α radiation, $\lambda=1.54178$ Å). Intensity data were collected using ω and ϕ scans spanning at least a hemisphere of reciprocal space for all structures (data were integrated using SAINT). Absorption effects were corrected on the basis of multiple equivalent reflections (SADABS). Structures were solved by direct methods (SHELXS^{S1}) and refined by full-matrix least-squares against F^2 (SHELXL^{S1}). Hydrogen atoms were assigned riding isotropic displacement parameters and constrained to idealized geometries, including those bound to oxygen, as no hydrogen atoms could be located in the difference Fourier map.

S3.1 X-Ray Crystal Structure of Handcuff Catenane HC•8PF₆

Crystals were grown by slow vapor diffusion of *i*-Pr₂O into a solution of HC•8PF₆ dissolved in MeCN. The presence of ‘flat’ and ‘torqued’ conformations of HC•8PF₆ are expressed in terms of disorder in the solid state. The crystal contains the ‘flat’ and ‘torqued’ conformations in a ratio of approximately, 7:3 respectively.

Crystal data for HC•8PF₆: C₁₁₀H₁₁₈N₈O₁₄•8(PF₆); purple prism, 0.191 × 0.174 × 0.096 mm³; monoclinic, space group $P2_1/c$; $a = 20.0951(4)$, $b = 31.3942(6)$, $c = 24.2862(5)$ Å; $\beta = 94.082(1)^\circ$; $V = 15282.6(5)$ Å³; $Z = 4$; $\rho_{\text{calcd}} = 1.276$ gcm⁻³; $T = 100(2)$ K; $R_1(F^2 > 2\sigma F^2) = 0.0893$; $wR_2 = 0.2511$. Out of 111556 reflections collected, a total of 25954 were unique. Crystallographic data (excluding structure factors) for the structures reported in this communication have been deposited with the Cambridge Crystallographic Data Center as supplementary publication no. CCDC–915345.

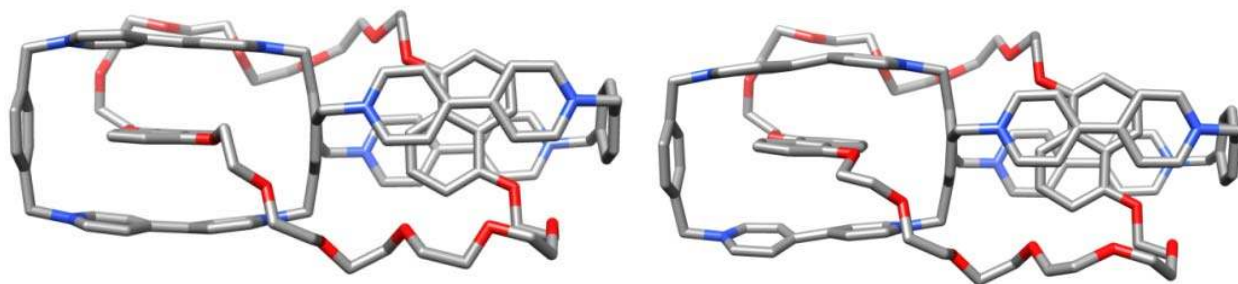


Figure S16. Crystal structure views left: ‘flat’ co-conformation, and right: ‘torqued’ co-conformation of HC•8PF₆. Hydrogen atoms omitted for the sake of clarity.

S3.2 X-Ray Crystal Structure of Ditopic Host **DBB**•8PF₆

Crystals were grown by slow vapor diffusion of *i*-Pr₂O into a solution of **DBB**•8PF₆ dissolved in MeCN.

Disordered PF₆⁻ anions were subjected to SADI restraints to effect an equivalent coordination environment around the P atom. Disordered and partially occupied MeCN solvent molecules were refined with SADI restraints to keep affected bonds equivalent. A global rigid bond (DELU) restraint was applied, and various SIMU restraints were applied to disordered PF₆⁻ and MeCN molecules. C24T C24S, N9S N9T C17T C18T C17S C18S, and N14S C27S C28S, were respectively refined with group displacement parameters. SOFs were allowed to refine freely, but were fixed (for the multiply-disordered PF₆⁻ and partially occupied MeCN) during the final refinement stages.

Crystal data for **DBB**•8PF₆: C₆₆H₅₈N₈•8(PF₆); 6.86(C₂H₃N); colorless needle, 0.269 × 0.055 × 0.04 mm³; triclinic, space group $P\bar{1}$; $a = 16.6223(5)$, $b = 22.9236(6)$, $c = 29.6344(8)$ Å; $\alpha = 71.154(2)$, $\beta = 78.075(2)$, $\gamma = 73.175(2)^\circ$; $V = 10149.1(5)$ Å³; $Z = 4$; $\rho_{\text{calcd}} = 1.574$ gcm⁻³; $T = 100(2)$ K; $R_1(F^2 > 2\sigma F^2) = 0.0983$; $wR_2 = 0.2597$. Out of 59810 reflections collected, a total of 24665 were unique. Crystallographic data (excluding structure factors) for the structures reported in this communication have been deposited with the Cambridge Crystallographic Data Center as supplementary publication no. CCDC-915343.

S3.3 X-Ray Crystal Superstructure of Inclusion Complex (**BHEEN**)₂ ⊂ **DBB**•8PF₆

Crystals were grown by slow vapor diffusion of *i*-Pr₂O into an MeCN solution containing **BHEEN** and **DBB**•8PF₆ in a ratio of 4:1, respectively.

Rigid bond restraints (esd 0.01) were imposed on the displacement parameters as well as restraints on similar amplitudes (esd 0.05) separated by less than 1.7 Å on the disordered fluorine and polyether chains. The disordered polyether chains were refined with distance restraints. Group anisotropic displacement parameters were refined for C79 C80 C79a C80a and also the C109 to O15 polyether chain. The solvent masking procedure as implemented in Olex2 was used to remove the electronic contribution of solvent molecules from the refinement. Only the atoms used in the refinement model are reported in the formula here. Total solvent accessible volume / cell = 487.7 Å³ [6.6%] Total electron count / cell = 77.2.

Crystal data for (**BHEEN**)₂ ⊂ **DBB**•8PF₆: C₆₆H₅₈N₈•8(PF₆), 2.5(C₁₈H₂₄O₆), 7(C₂H₃N); purple block, 0.153 × 0.115 × 0.066 mm³; triclinic, space group $P\bar{1}$; $a = 16.475(4)$, $b = 18.609(5)$, $c = 25.278(6)$ Å, $\alpha = 105.106(8)$, $\beta = 99.281(7)$, $\gamma = 93.008(6)^\circ$; $V = 7348(3)$ Å³, $Z = 2$; $\rho_{\text{calcd}} = 1.469$ gcm⁻³; $T = 100(2)$ K; $R_1(F^2 > 2\sigma F^2) = 0.0668$; $wR_2 = 0.1811$. Out of 58131 reflections collected, a total of 23976 were unique. Crystallographic data (excluding structure factors) for the

structures reported in this communication have been deposited with the Cambridge Crystallographic Data Center as supplementary publication no. CCDC-915344.

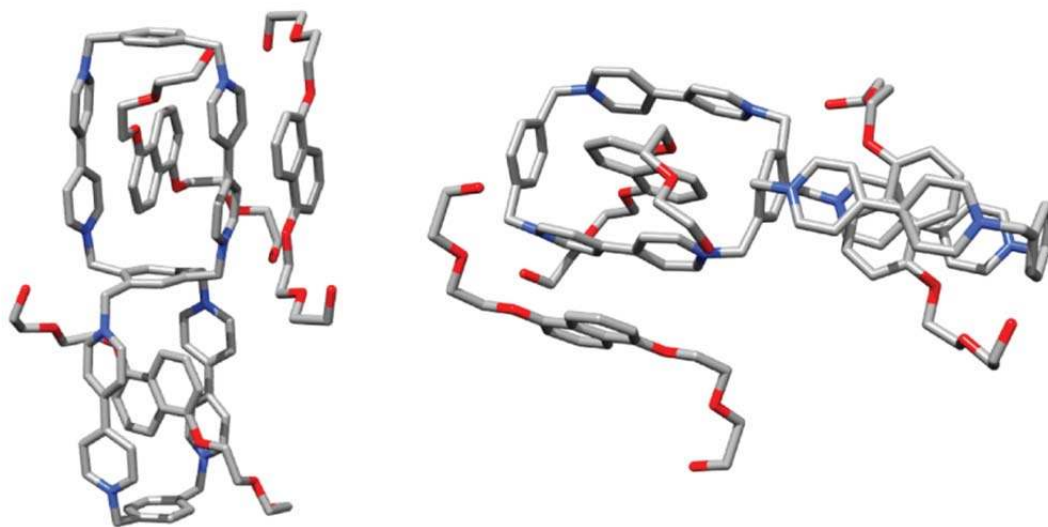


Figure S17. Crystal superstructure views of $(\text{BHEEN})_2 \cdot \text{DBB} \cdot 8\text{PF}_6$.
Hydrogen atoms omitted for the sake of clarity.

S4. Quantum Mechanical Calculations

Density Functional Theory (DFT) calculations were performed with the B3LYP-D3 exchange-correlation functional^{S2} using the Jaguar^{S3} software package run in parallel on multiple processors. The pseudospectral^{S4} methodology, which speeds up the SCF iterations significantly, was employed for all calculations. Ultra-fine DFT grids as implemented in Jaguar (specified with the keywords `gdftmed=-13`, `gdftfine=-13` and `gdftgrad=-13`) were used for the calculations to improve the structural convergence during the geometry optimizations. All structures were optimized with the 6-31G** basis set in vacuum. Single-point calculations on the B3LYP-D3/6-31G** optimized structures were then performed with the larger 6-311G**++ basis set, while estimates for the solvation energies were computed with either the continuum Poisson Boltzman^{S3} or the SM8^{S5} solvent model implemented in Jaguar using solvent parameters for dimethylformamide at the B3LYP-D3/6-31G** level.

The calculated results indicate that in vacuum, the two topologies (*meta-meta*, co-conformation 2 and *ortho-ortho*, co-conformation 1) have very similar energies, which differ by less than 2.5 kcal/mol. Solvation seems to favour the experimentally preferred *meta-meta* isomer by several kcal/mol, however, with both solvation models (see Table S1).

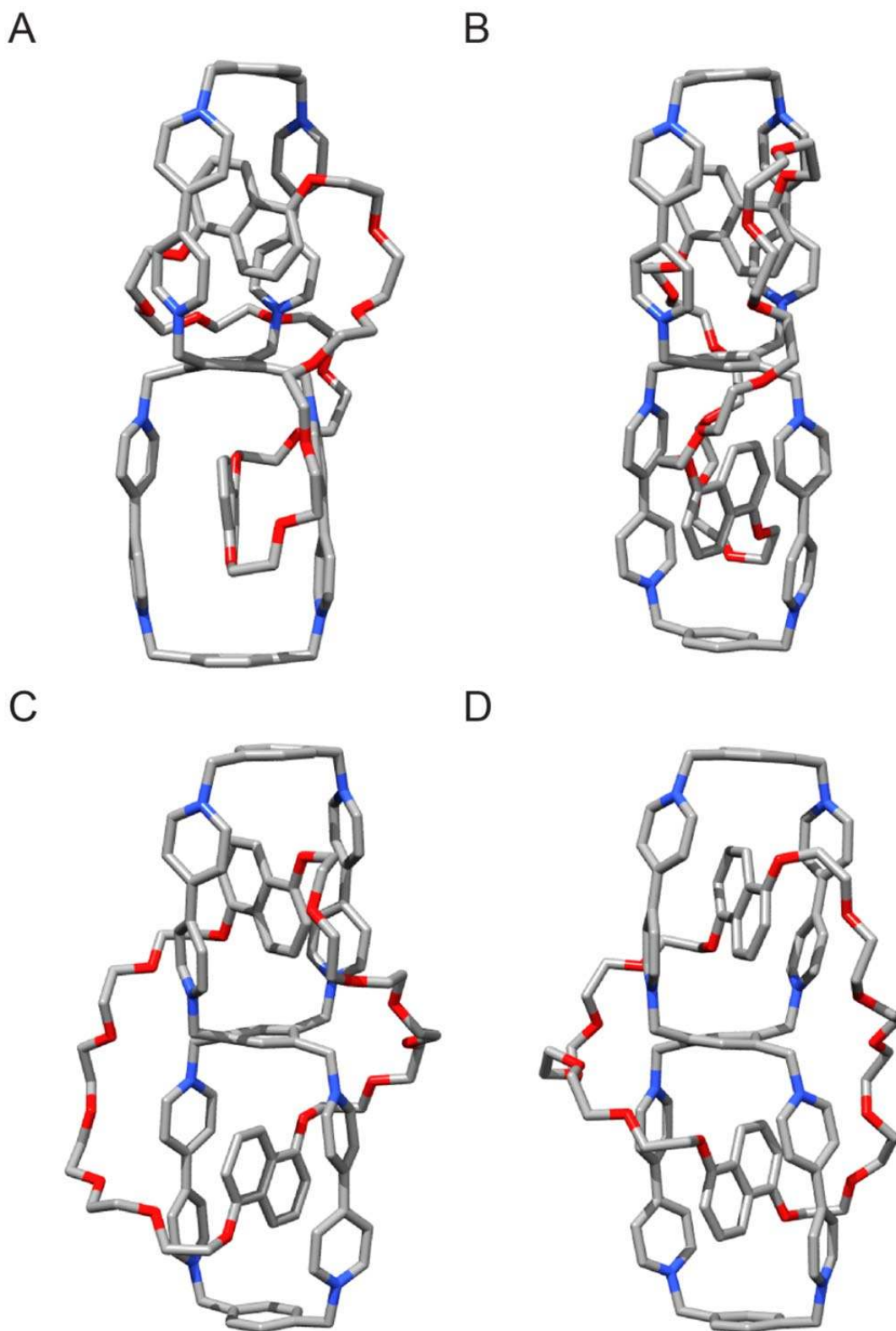


Figure S18. DFT-optimized structures of a) *meta-meta* isomer, co-conformation 1, b) *meta-meta* isomer, co-conformation 2, the experimentally observed structure, c) *ortho-ortho* isomer, co-conformation 1 and b) *ortho-ortho* isomer, co-conformation 2.

S4.1. DFT-Optimized Structures and Energies

The four different structures considered for DFT calculations are shown in Figure S18. These structures were chosen based on the two possible topologies – *meta-meta* and *ortho-ortho* – as well as the two possible combinations of DNP orientations within each cyclophane – co-conformations 1 and 2. Co-conformation 2 is the co-conformation that is observed by single-crystal X-ray diffraction.

Table S1. Relative Computed DFT-Energies (in kcal/mol) of the different Handcuff-Catenane Topologies.

	In Vacuum^a	PBF Solvation^b	SM8 Solvation^c
(A) <i>Meta-Meta</i> isomer, Co-conformation 1	14.36	16.24	5.51
(B) <i>Meta-Meta</i> isomer, Co-conformation 2 (experimentally observed topology)	0.00	0.00	0.00
(C) <i>Ortho-Ortho</i> isomer, Co-conformation 1	-2.44	5.94	2.37
(D) <i>Ortho-Ortho</i> isomer, Co-conformation 2	6.40	10.23	7.61

^a B3LYP-D3/6-311G**++//B3LYP-D3/6-31G** level. ^b Vacuum energies + solvation energies computed at the B3LYP-D3/6-31G** level with the Poisson-Boltzman solvation model. ^c Vacuum energies + solvation energies computed at the B3LYP-D3/6-31G** level with the SM8 solvation model.

S5. Analytical Reverse-Phase HPLC

Analytical reverse-phase HPLC was used to determine the purity of both the handcuff catenane **HC**⁸⁺ (Figure S19) and the ditopic host **DBB**⁸⁺ (Figure S20). Figure S19 shows a single peak in the chromatogram, indicating that the *meta-meta* and *ortho-ortho* isomers have very similar retention times. The two topological isomers could not be separated using HPLC techniques.

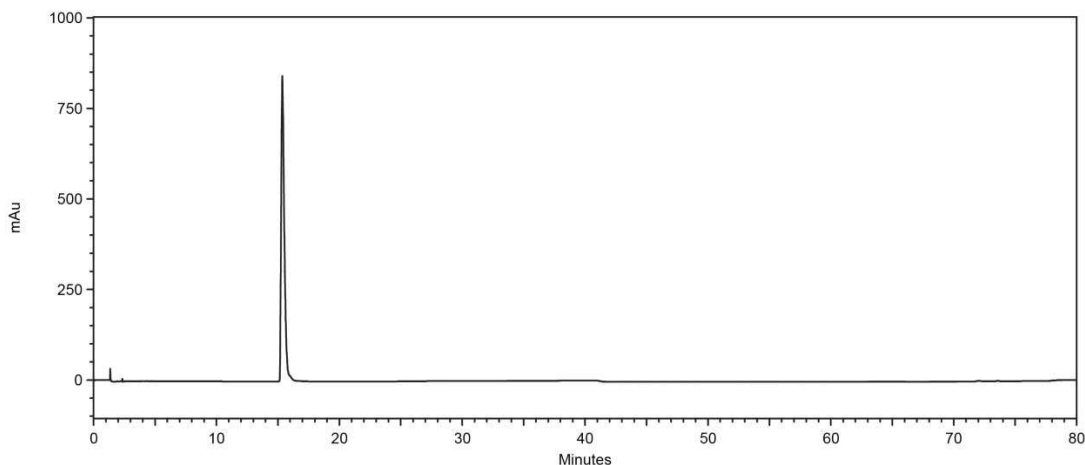


Figure S19. Analytical RP-HPLC trace (H₂O/0.1% TFA – MeCN/0.1% TFA, 0 – 50% in 65 mins → 100% MeCN/0.1% TFA after 80 mins) of handcuff catenane **HC**•8PF₆. The single peak represents two topological isomers.

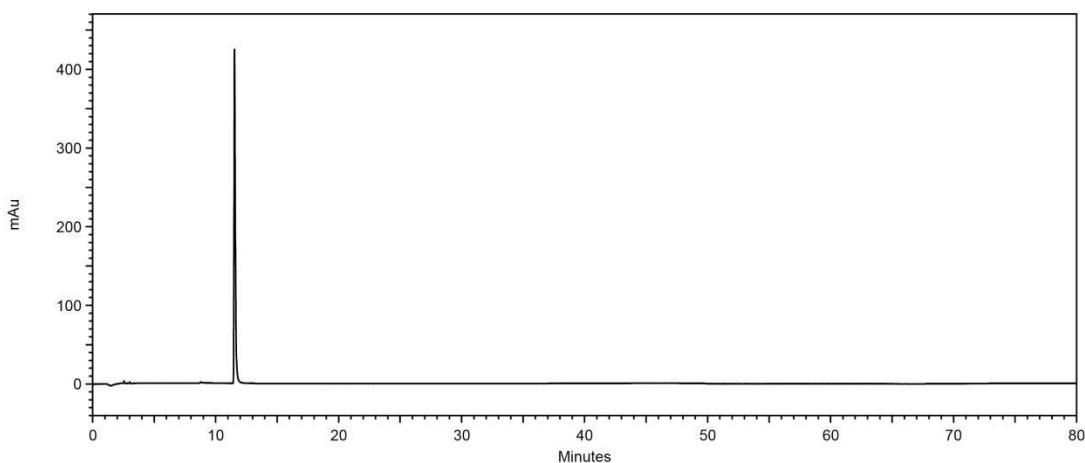


Figure S20. Analytical RP-HPLC trace (H₂O/0.1% TFA – MeCN/0.1% TFA, 0 – 50% in 65 mins → 100% MeCN/0.1% TFA after 80 mins) of **DBB**•8PF₆.

S6. Isothermal Titration Calorimetry (ITC)

ITC measurements (Figure S21) were performed in dry, degassed MeCN at 298 K. A solution of **DBB**·8PF₆ (0.75 mM) was used as the host solution. Solutions of **BHEEN** (15 mM) were added by injecting 5 μL of a titrant solution over 20 s, which was repeated 50 times with a 300 s interval between each injection. Experiments were repeated three times. Thermodynamic parameters were calculated using a sequential binding site model utilizing data from which the heat of dilution of **BHEEN** was subtracted, with the average of three runs reported, and the error represents the standard deviation calculated from those runs.

$$\begin{aligned}K_1 &= 2047 \pm 249 \text{ M}^{-1} \\ \Delta H_1 &= -13.8 \pm 0.7 \text{ kcal} \cdot \text{mol}^{-1} \\ \Delta S_1 &= -31.3 \pm 0.6 \text{ cal} \cdot \text{mol}^{-1} \cdot \text{K}^{-1} \\ \Delta G_1 &= -4.5 \pm 0.5 \text{ kcal} \cdot \text{mol}^{-1}\end{aligned}$$

$$\begin{aligned}K_2 &= 52 \pm 6 \text{ M}^{-1} \\ \Delta H_2 &= -34.8 \pm 6.5 \text{ kcal} \cdot \text{mol}^{-1} \\ \Delta S_2 &= -109 \pm 18.7 \text{ cal} \cdot \text{mol}^{-1} \cdot \text{K}^{-1} \\ \Delta G_2 &= -2.3 \pm 0.3 \text{ kcal} \cdot \text{mol}^{-1}\end{aligned}$$

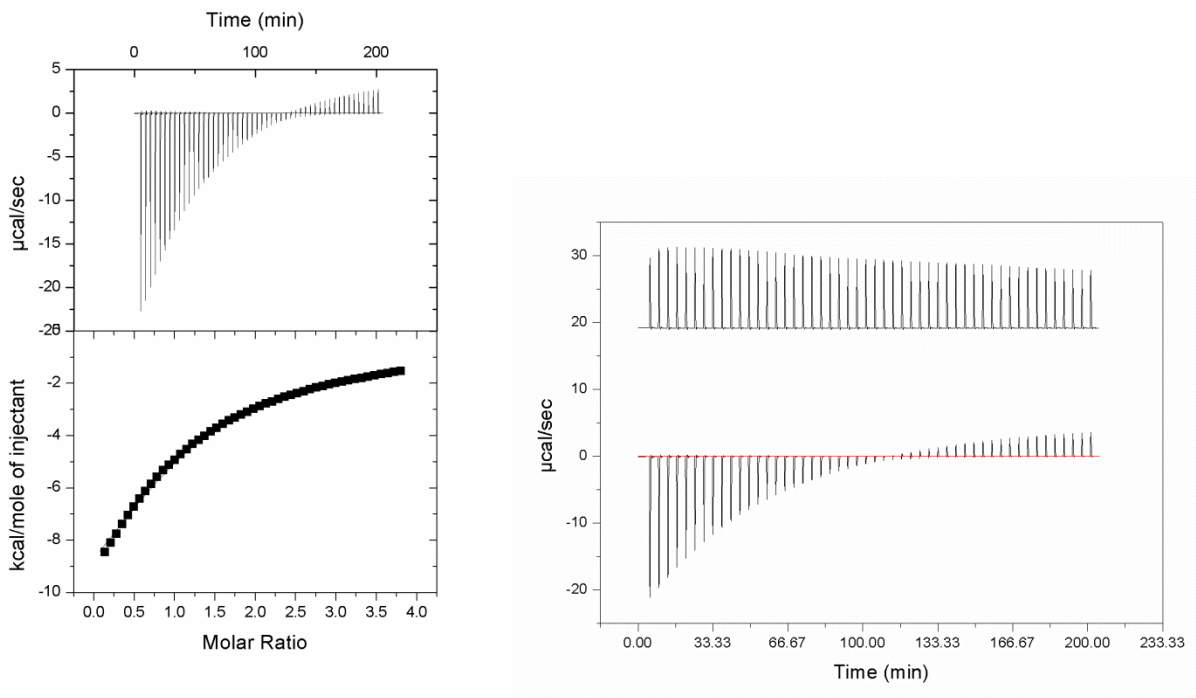


Figure S21. a) ITC trace of the (**BHEEN**)₂ ⊂ **DBB**·8PF₆ complex, b) ITC trace revealing large endothermic heat of dilution upon addition of **BHEEN** to MeCN.

S7. References

- (S1) G. Sheldrick, *Acta Crystallogr. Sect. A*, 2008, **64**, 112–122.
- (S2) a) A. D. Becke, *J. Chem. Phys.*, 1993, **98**, 5648–5652; b) C. T. Lee, W. T. Yang, and R. G. Parr, *Phys. Rev. B*, 1988, **37**, 785–789; c) P. J. Stephens, F. J. Devlin, C. F. Chabalowski, and M. J. Frisch, *J. Phys. Chem.*, 1994, **98**, 11623–11627; d) S. H. Vosko, L. Wilk, and M. Nusair, *Canad. J. Phys.*, 1980, **58**, 1200–1211; e) S. Grimme, J. Antony, S. Ehrlich, and H. Krieg, *J. Chem. Phys.*, 2010, **132**, 154104.
- (S3) Jaguar, Version 7.9; Schrödinger, LLC, New York (USA), **2012**.
- (S4) a) R. A. Friesner, *Chem. Phys. Lett.*, 1985, **116**, 39–43; b) R. A. Friesner, *J. Chem. Phys.*, 1986, **85**, 1462–1468; c) R. A. Friesner, *J. Chem. Phys.*, 1987, **86**, 3522–3531; d) R. A. Friesner, *J. Phys. Chem.*, 1988, **92**, 3091–3096.
- (S5) a) A. V. Marenich, R. M. Olson, C. P. Kelly, C. J. Cramer, and D. G. Truhlar, *J. Chem. Theory Comput.*, 2007, **3**, 2011–2033. b) R. M. Olson, A. V. Marenich, C. J. Cramer, and D. G. Truhlar, *J. Chem. Theory Comput.*, 2007, **3**, 2046–2054.